Double Noise Filtering in CT: Pre- and Post-Reconstruction

Vinicius C. Assis[1], Denis H. P. Salvadeo[1], Nelson D. A. Mascarenhas[2], Alexandre L. M. Levada[3]
[1]State University of São Paulo, Department of Statistics, Applied Mathematics and Computing, Rio Claro SP, Brazil
[2]Faculdade Campo Limpo Paulista, Graduate Program in Computer Science, Campo Limpo Paulista SP, Brazil
[3]Federal University of São Carlos, Department of Computing, São Carlos SP, Brazil
{vcovre, salvadeo}@rc.unesp.br, nelson@cc.faccamp.br, alexandre@dc.ufscar.br

***Abstract*—Motivated by the ALARA (As Low As Reasonably Achievable) principle, this paper proposes to denoise Computed Tomography (CT) images by using a double-filtering approach. First, projection data were filtered using methods to filter Poisson noise (pre-filtering step). Then the filtered backprojection (FBP) algorithm was applied to image reconstruction. After, the reconstructed images were denoised by using suitable methods for filtering Gaussian noise (post-filtering step). Finally, known metrics of image quality evaluation (such as SSIM and PSNR) were used to compare the filtered images with the ones considered ideal images in various combinations of filters. The results lead to the conclusion that a second filtering applied on image domain can improve the CT denoising quality from pre-filtering step. Thus, CT double-filtering strategy achieved a better balance between noise reduction and details preservation.**

***Keywords*-Computed Tomography (CT); Double Denoising.**

I. Introduction

In order to avoid an invasive analysis in the patient, Computed Tomography (CT) was established as a method of obtaining internal images of a body (or object) by emitting X-ray or γ-ray. This two-dimensional image of a three-dimensional body is represented as a slice in which the rays goes from the emissor to the detector, crossing the body.

Traditionally, CT is associated with medical diagnosis. However, this technique of imaging has applications in many other areas, such as agriculture and industry.

The data obtained by the radiation detector are known as projection data whose noise follows Poisson statistics: a signal-dependent noise [1], [2] characterized by having the same mean and variance. Furthermore, the projection data has Poisson noise due to the low photon counting [3].

Then, a reconstruction method is applied in projection data to generate an image of the slice of the body/object in analysis.

In addition, the reconstructed CT image noise can be approximated by a zero-mean, signal-dependent Gaussian noise [4] (by invoking the Central Limit Theorem [2]).

Thus, in accordance with the ALARA principle (As Low As Reasonably Achievable) [4] which establishes the idea that radiation doses should be the lowest possible for a suitable exam acquisition (in order to reduce radiation emission for CT), this paper proposes to use a double denoising method to filter noisy CT data acquired on low radiation dose, in order to get a better balance between details preservation and noise reduction.

Basically, a double-filtering in this research is to filter the projection data (pre-filtering), rebuild them and then apply a new filtering stage (post-filtering), but now on the reconstructed image.

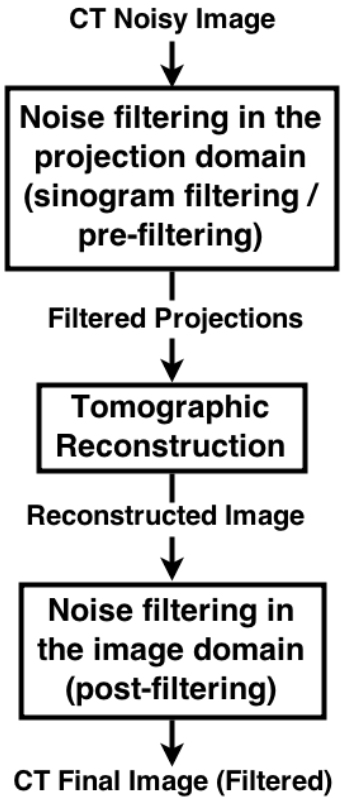

Fig. 1. Block diagram for CT double-filtering

Some related works using double-filtering for CT images can be found in the literature [5], [6]. The work [6] uses a Penalized Weighted Least-Squares approach with Karhunen-Loève (KL-PWLS) to filter sinogram and a NLM approach for image domain filtering. On the other hand, [5] uses Kalman filter for pre-filtering step and Wavelet Shrinkage for post-filtering step.

Contributions: In summary, the contribution of this paper is a comprehensive study of double noise filtering in CT, in order to take the best advantages of both filtering methods,

by using state-of-art and classical methods to filter Poisson noise in CT projections and Gaussian noise in reconstructed image. Its main goal is to reduce noise levels on CT images respecting ALARA philosophy.

This paper is organized as follows. Section II presents the methodology of this work and also describes the methods used to develop the proposed idea. Section III discusses the experimental considerations and the results are shown in Section IV. Finally, the conclusions and future work are discussed in Section V.

II. Methodology

As previously mentioned, our study consists of CT double denoising, filtering both (pre- and post-) reconstruction steps, as illustrated in Fig. I.

In the experiments, the projection data were acquired with different exposure times of tomograph rays, which gave us images that we consider as ideal (20 seconds of exposure) and noisy (3 seconds of exposure).

Anscombe Tranform: Given the fact that the Poisson noise is signal-dependent, Anscombe Transform (AT) [7] aims to stabilize the variance of the noise. It is able to transform a dependent noise signal to an additive noise, approximately Gaussian, with zero mean and unit variance. Thus, it is common to see the pre-filters working in Anscombe domain, and after the process, the inverse Anscombe Transform (IAT) is applied, so that the image is ready to go trough a reconstruction process.

So, for filtering this kind of data (pre-filtering step), whose noise follows a Poisson distribution [8], the pre-filters used were: Pointwise Wiener filter (1D-PWF) [9], tradicional Non-Local Means (AT-NLM) [10] and a version for Poisson noise (P-NLM) [3], Maximum a Posteriori (MAP) [8], Block-Matching and 3D filtering (AT-BM3D) [11] and contextual versions of the Wiener filter based on Markov Random Fields (MRF), such as Generalized Wiener filter (AT-GWF) [12] and Wiener filter with Isotropic (AT-IWF) and Separable (AT-SWF) [13] MRF. All these filters were applied on Anscombe Domain, except for the MAP and P-NLM.

After a pre-filtering, the filtered data goes trough a mathematical method for image reconstruction. For this paper, the traditional Filtered Backprojection (FBP) algorithm [1] was used.

The filtering in image domain is known as post-filtering, and for those, we investigated: 2D-PWF [9], NLM [10], GWF [12], BM3D [11] and also the filters IWF and SWF [13].

In the following Subsections, we present a brief description of the filters used in our study.

A. Pointwise Wiener Filter (PWF)

Defined as a linear minimum mean square error (LMMSE) estimate [9] of a desired signal from a noisy, the PWF filter is a traditional method of filtering in CT.

This noise reduction method has its process defined by the following equation:

$$g_s = f_s + v_s, \tag{1}$$

where g_s is the observed noisy signal, f_s the noise-free signal and v_s is the noise at s pixel.

The Pointwise version of this filter is proposed by [9], with the following equation:

$$\hat{f}_s = \mu_{f_s} + \frac{\sigma^2_{f_s}}{\sigma^2_{f_s} + \sigma^2_{v_s}} \left(g_s - \mu_{g_s}\right). \tag{2}$$

where μ_{f_s} is the local mean of f and $\sigma^2_{f_s}$ and $\sigma^2_{v_s}$ are the local variances of the original image f and the noise v, respectively.

Finally, it is important to mention that the 1D version (1D-PWF) [8] obtains the image statistics (mean and variance) by using a 1D window, while 2D-PWF uses a 2D one.

B. Generalized Wiener Filter (GWF)

Also known as Wiener filter with Fisher information [12], it is a derivation of the just mentioned method where Fisher information represents the data quantity which a random variable has under the parameter to be estimated. This filter is described by:

$$\begin{aligned}\hat{f}_s = \mu_{f_s} &\\ + \frac{\sigma^2_{f_s}}{\sigma^2_{f_s} + \sigma^2_{v_s}} &\big[\alpha(g_s - \mu_{f_s}) \\ + (1-\alpha) &\sum_{g_t \in \eta_s} (g_t - \mu_{g_s})\big],\end{aligned} \tag{3}$$

where α controls the context level to be considered in the estimation of the noise-free pixel and g_t is a neighbor pixel in the neighborhood η_s of s.

C. Pointwise - Maximum a Posteriori (MAP)

The method is a way to obtain the signal pointwise estimator which has a great performance when known this signal statistics. According to [8] a MAP estimator regarding Poisson and Gaussian as likelihood and a priori distributions, respectively, is given by the equation:

$$\hat{f}_s = \frac{\mu_{g_s} - \sigma^2_{g_s}\sqrt{(\sigma^2_{g_s} - \mu_{g_s})^2 + 4\sigma^2_{g_s} g_s}}{2}. \tag{4}$$

D. Non-Local Means (NLM)

Due to patch (P) redundancies in an image, NLM [10] was created to incorporate this information into denoising. Basically, the original estimated value is given by the weighted average of noisy pixels in a region. Traditionally, the weights of its averages are obtained by the Euclidean distance to measure similarity between the central and the neighbor patches. The following equation

$$\hat{f}_s = \frac{\sum_{t \in W} \omega(s,t) g_t}{\sum_{t \in W} \omega(s,t)}, \tag{5}$$

represents the method, where to get noise-free estimation of an image pixel ($\hat{f}_s$), W represents a search window, g_t is a noisy pixel in this window and $\omega(s,t)$ are the weights corresponding

to the similarity between patches centered at s and t. The weights are defined by the formula:

$$\omega(s,t) = \exp\left(-\frac{1}{h}\sum_{k\in P}|g_{s,k} - g_{t,k}|^2\right), \quad (6)$$

where the parameter h controls the smoothing, and $g_{s,k}$ and $g_{t,k}$ are k-th elements of the noisy patches at s and t, respectively.

As the Euclidean distance is suitable for additive white Gaussian noise (AWGN), P-NLM [3] is an adapted version of NLM, but for Poisson noise. The main modification consists in changing the similarity measure in order to get a more suitable one for Poisson noise.

E. Block-Matching and 3D filtering (BM3D)

It is an state-of-art denoising method which does the similar block matching (2D), accumulating them in 3D groups.

BM3D [11] preserves well the textures, repeated areas, uniform areas, edges (even the thin ones) and singularities. However, the main problem is the addition of artifacts to the images.

The idea of using BM3D as a pre-filter in Anscombe Domain (AT-BM3D) was inspired by [14], [15]. In [14], BM3D was applied for the first time on the Anscombe Domain to evaluate the proposal of an exact inverse Anscombe Transform. In turn, [15] applied it to denoise Positron Emission Tomography (PET).

F. Wiener filters with Isotropic (IWF) and Separable (SWF) MRF

Supposing a lexicographic notation, $\hat{f}$ is a window estimative of the original N pixels image, defined as a linear combination of g, given by

$$\hat{f} = \sum_{n=0}^{N-1}\alpha_n g[n] \quad (7)$$

where α_n are the weights which minimize $\epsilon = f - \hat{f}$ and g is the pixel of a noisy image. This is the same as minimizing the expected value of $||\epsilon||^2$, obeying the Orthogonality Principle [13].

This way, we get a system of N equations with N unknowns, admitting only one solution, as described by

$$R_{gg}\alpha = R_{fg}, \quad (8)$$

Moreover, it is important to mention that each line of R_{gg} matrix represents the autocorrelation of g pixels between each pixel and each other point of a window, while R_{fg} is a vector which represents the autocorrelation of f pixels from the center point (current) and all other observed values of the window.

For SWF, the autocorrelation matrices for each central pixel (i,j) in a $W \times W$ window are:

$$R_{gg} = \begin{cases}\sigma_f^2(i,j) + \sigma_v^2(i,j), & \text{main diagonal}\\ \sigma_f^2(i,j)\rho_V^{|i'-i''|}\rho_H^{|j'-j''|}, & \text{remainder}\end{cases} \quad (9)$$

$$R_{ff} = (\sigma_f^2(i,j)\rho_V^{|i'-i|}\rho_H^{|j'-j|}); \quad (10)$$

where ρ_V and ρ_H are vertical and horizontal correlation coefficients, both valued 0.95, and (i',j') and (i'',j'') correspond to pixels positions in a window.

On the other hand, we have for IWF:

$$R_{gg} = \begin{cases}\sigma_f^2(i,j) + \sigma_v^2(i,j), & \text{main diagonal}\\ \sigma_f^2(i,j)\rho^{\sqrt{(i'-i'')^2+(j'-j'')^2}}, & \text{remainder}\end{cases} \quad (11)$$

$$R_{ff} = (\sigma_f^2(i,j)\rho^{\sqrt{(i'-i)^2+(j'-j)^2}}), \quad (12)$$

where ρ is a correlation coefficient, also valued 0.95.

III. Experimental Evaluation

For our experiments, it is necessary to reinforce some topics: (*i*) we used Matlab software for implementations; (*ii*) there was a visual evaluation and also quantitative, by using Peak Signal-to-Noise Ratio (PSNR) and Structural Similarity Index (SSIM) [16] comparing the final images, after the reconstruction process; (*iii*) comparisons were made with double-filtering and also with pre- and post-filtering only; (*iv*) standard deviation of the images were manually obtained by selecting a constant area of each image and taking notes; (*v*) the standard deviations of the noisy images and also of the pre-filtered ones (used only for post-filtering) are in Table I.

TABLE I
Standard Deviations Parameters

Methods	Standard Deviation	
	Image 1	Image 2
Noisy Image	22.4	16.2
MAP	19.3	8.8
P-NLM	26.5	9.6
AT-NLM	20.3	16.3
AT-BM3D	11.6	5.7
1D-PWF	21.6	4.0
AT-GWF	15.2	10.6
AT-IWF	12.8	14.1
AT-SWF	19.5	13.6

IV. Results

The filtered images obtained by using the proposal are displayed in Figs. 2 to 7 and the results in terms of PSNR and SSIM are shown in Tables II to IV, comparing ideal images (exposed to 20 seconds of radiation) with filtered noisy images (exposed to 3 seconds of radiation). The ideal and noisy images used in these experiments are displayed in Figs. 2 (items a and b) and 3 (items a and b) for Image 1 and 2, respectively. In addition, these results are discussed in next Subsections.

A. Pre-Filtering

According to Table II and Figs. 2 and 3, AT-BM3D has the best SSIM results while AT-GWF has the best PSNR results. Although visually having a superior reduction of noise levels comparing with AT-GWF, AT-BM3D added some artifacts in the images.

In the second place, the NLM for Poisson noise (P-NLM) also obtained interesting results, as well as 1D-PWF, AT-IWF and AT-SWF.

In addition, we compared the higher quantitative results with the second ones. A pre-filtering using AT-GWF improved in terms of PSNR around 0.1 dB for Image 1 in comparison with AT-IWF and 0.98 dB comparing with AT-BM3D for Image 2. For SSIM results, AT-BM3D improved 0.05 comparing with P-NLM for Image 1 and 0.02 in comparison with AT-GWF for Image 2.

Finally, MAP and AT-NLM underperformed the methods above, displaying a low Signal-to-Noise Ratio (SNR).

TABLE II
PSNR AND SSIM RESULTS FOR PRE-FILTERING

Methods	Image 1		Image 2	
	PSNR (dB)	**SSIM**	**PSNR (dB)**	**SSIM**
Noisy Image	15.91	0.27	19.88	0.56
MAP	17.79	0.33	22,17	0.62
P-NLM	20.25	0.43	24.47	0.63
AT-NLM	16.79	0.31	20.46	0.49
AT-BM3D	18.89	**0.48**	24.90	**0.72**
1D-PWF	20.08	0.40	22.54	0.64
AT-GWF	**20.52**	0.42	**25.88**	0.70
AT-IWF	20.45	0.42	21.65	0.62
AT-SWF	19.53	0.41	21.95	0.64

B. Post-Filtering

In quantitative terms (Table III), as well as in qualitative terms for post-filtering displayed in Figs. 4 and 5, the best results appeared when applied BM3D filter. Visually, a better balance between noise reduction and detail preservation was achieved comparing with any other applied method but yet adding some artifacts in the images.

It is believed that the addition of artifacts when using AT-BM3D and BM3D is because of the patch shape, specially in the pre-filtering case. The data above and below the sinogram line do not correspond to the neighbor pixels in image domain. Thus, patch shape should be defined in the projection line (1-D) and not squared (2-D), as it is implemented.

As a result of the BM3D post-filtering, there was an improvement of 0.19 dB and 0.12 dB for Images 1 and 2 respectively, comparing with IWF and SWF in terms of PSNR. Conversely, SSIM improved in 0.02 comparing with both IWF and SWF for Image 1, while Image 2 filtered with BM3D and SWF achieved the same values.

Secondly, similar results are obtained in SWF, IWF and GWF (for PSNR and SSIM). Lastly, 2D-PWF and NLM did not achieve so interesting visual results, because of excessive smoothing.

In addition, it is noteworthy that post-filters are inferior than pre-filters, in qualitative and quantitative evaluations.

C. Double-filtering

For double-filtering, the results are shown in Table IV and Figs. 6 and 7. It is noteworthy that Table IV follows the name pattern: $X + Y$, where pre-filters and post-filters are represented by X and Y, respectively.

Moreover, the lines and columns in Figs. 6 and 7 represent the pre-filters applied to noisy CT images and post-filters applied to the pre-filtered data, respectively.

TABLE III
PSNR AND SSIM RESULTS FOR POST-FILTERING

Methods	Image 1		Image 2	
	PSNR (dB)	**SSIM**	**PSNR (dB)**	**SSIM**
Noisy Image	15.91	0.27	19.88	0.56
NLM	16.23	0.26	19.22	0.47
BM3D	**17.28**	**0.37**	**21.05**	**0.64**
2D-PWF	16.26	0.26	19.45	0.50
GWF	16.95	0.34	20.75	0.63
IWF	17.09	0.35	20.93	0.63
SWF	17.09	0.35	20.93	**0.64**

Thereby, after all double denoising evaluations, it is clear that using a post-filtering in the pre-filtered data projection considerably improves the results in general, comparing to the only pre-filtered results.

Concerning a comparison between a pre-filter application and double-filtering with the same pre-filter, the results improved in general when applied a post-filter to the pre-filtered image. However, the use of 2D-PWF and NLM decreased some results, mainly for Image 2.

For instance, a double-filtering using MAP, P-NLM, AT-NLM, AT-BM3D, 1D-PWF and AT-SWF improved an average of 1.08 dB, 0.98 dB, 0.82 dB, 1.31 dB, 1.06 dB and 0.67 dB respectively in terms of PSNR for Image 1 (AT-GWF and AT-IWF did not improve). In SSIM comparison, MAP, P-NLM, AT-NLM, AT-BM3D, 1D-PWF, AT-GWF, AT-IWF and AT-SWF achieved an enhancement of average 0.05, 0.02, 0.00, 0.04, 0.01, 0.01 and 0.02 for Image 1.

The Image 2, for example, improved in terms of PSNR in all methods except AT-BM3D and AT-GWF. On the other hand, SSIM results were worse in the comparison with only pre-filters, except the AT-NLM which improved an average of 0.08 and AT-IWF kept the same result in average.

Finally, the best improvements comparing with the noisy images is described as follows. In terms of PSNR, this is obtained by combining AT-GWF + BM3D for Image 1 (6.05 dB) and Image 2 (6.52 dB). On the other hand, in terms of SSIM, AT-BM3D + BM3D and AT-BM3D + SWF performed the highest results for Image 1 (0.22) and the pre-filter AT-BM3D for Image 2 (0.16).

V. CONCLUSION

In this paper, we proposed a review and comparison of the pre-filters, post-filters and double-filters, with CT applications. In other words, the denoising methods were used to filter both Poisson (in projection domain) and Gaussian (in image domain) noises.

In addition, to our knowledge, the proposal to use contextual Wiener filters and BM3D on Anscombe Domain to denoise CT was applied for the first time. They achieved a good quality outcome data.

The experiments were performed by using state-of-art methods and classical for each step. They show good results in general, improving quantitatively and qualitatively the resulting images, when compared to pre-filtering.

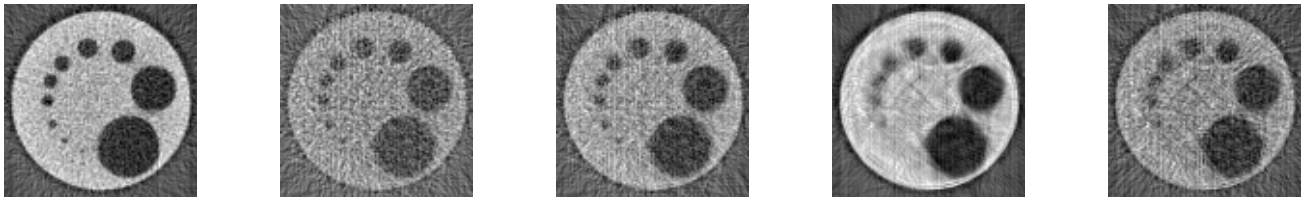

(a) Ideal (20s) (b) Noisy (3s) (c) MAP (d) P-NLM (e) AT-NLM

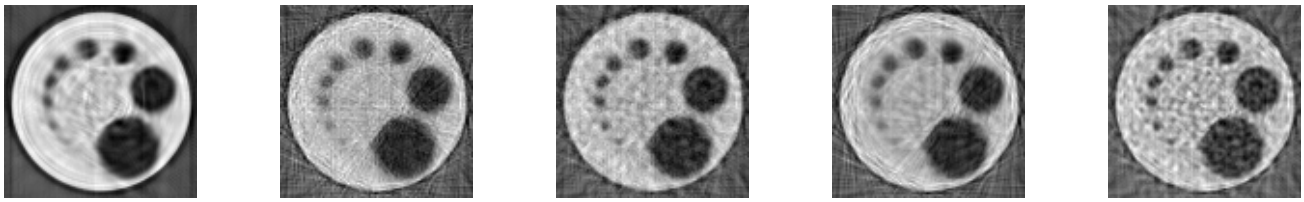

(f) AT-BM3D (g) 1D-PWF (h) AT-GWF (i) AT-IWF (j) AT-SWF

Fig. 2. Original Image, Noisy Image and Results of pre-filtering for Image 1

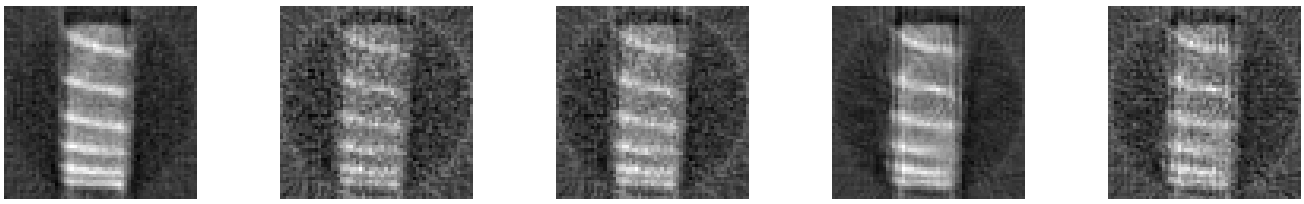

(a) Ideal (20s) (b) Noisy (3s) (c) MAP (d) P-NLM (e) AT-NLM

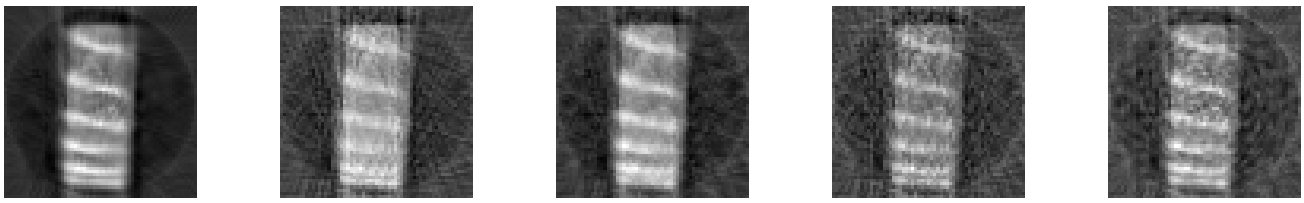

(f) AT-BM3D (g) 1D-PWF (h) AT-GWF (i) AT-IWF (j) AT-SWF

Fig. 3. Original Image, Noisy Image and Results of pre-filtering for Image 2

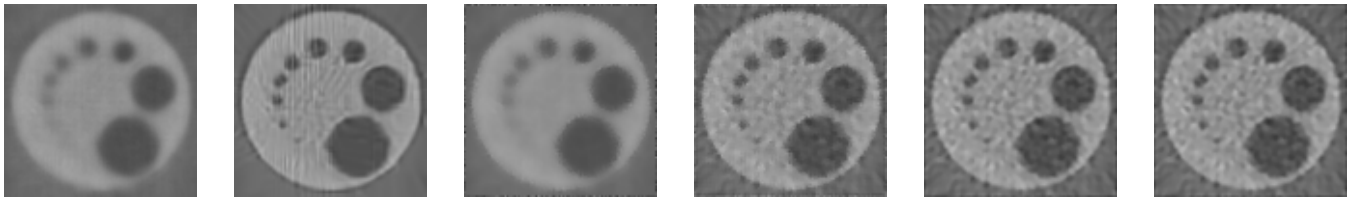

(a) NLM (b) BM3D (c) 2D-PWF (d) GWF (e) IWF (f) SWF

Fig. 4. Results of post-filtering for Image 1

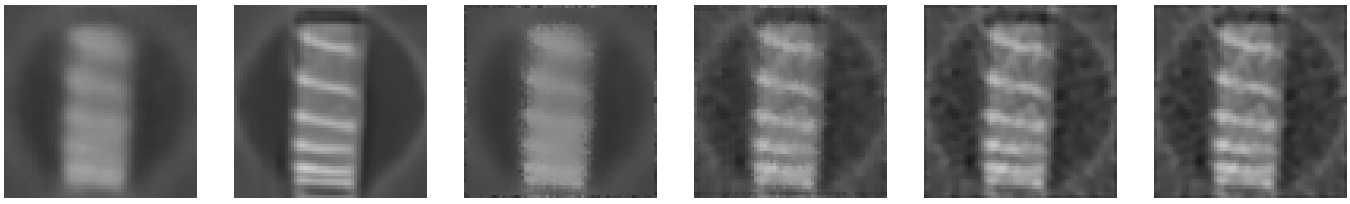

(a) NLM (b) BM3D (c) 2D-PWF (d) GWF (e) IWF (f) SWF

Fig. 5. Results of post-filtering for Image 2

TABLE IV
PSNR AND SSIM RESULTS FOR DOUBLE-FILTERING

Methods	Image 1		Image 2	
	PSNR (dB)	**SSIM**	**PSNR (dB)**	**SSIM**
Noisy Image	15.91	0.27	19.88	0.56
MAP + NLM	18.13	0.33	20.98	0.50
MAP + BM3D	19.53	0.43	23.47	0.67
MAP + 2D-PWF	18.29	0.34	21.70	0.57
MAP + GWF	18.96	0.39	22.99	0.65
MAP + IWF	19.14	0.40	23.24	0.67
MAP + SWF	19.15	0.40	23.25	0.68
P-NLM + NLM	21.18	0.44	22.86	0.53
P-NLM + BM3D	21.50	0.48	25.72	0.65
P-NLM + 2D-PWF	21.17	0.44	23.70	0.57
P-NLM + GWF	21.21	0.46	25.03	0.63
P-NLM + IWF	21.14	0.46	25.72	0.66
P-NLM + SWF	21.16	0.46	25.72	0.66
AT-NLM + NLM	17.07	0.31	20.42	0.49
AT-NLM + BM3D	18.10	0.41	22.27	0.62
AT-NLM + 2D-PWF	17.15	0.32	20.64	0.50
AT-NLM + GWF	17.71	0.37	21.93	0.60
AT-NLM + IWF	17.82	0.38	22.08	0.61
AT-NLM + SWF	17.83	0.38	22.08	0.61
AT-BM3D + NLM	19.51	0.47	22.58	0.56
AT-BM3D + BM3D	19.24	**0.49**	24.81	0.67
AT-BM3D + 2D-PWF	19.51	0.48	24.48	0.65
AT-BM3D + GWF	19.39	0.48	23.99	0.65
AT-BM3D + IWF	19.12	0.50	24.82	**0.69**
AT-BM3D + SWF	19.11	**0.49**	24.87	**0.69**
1D-PWF + NLM	20.63	0.41	21.54	0.51
1D-PWF + BM3D	21.69	0.47	23.17	0.64
1D-PWF + 2D-PWF	20.78	0.41	22.22	0.59
1D-PWF + GWF	21.16	0.44	22.94	0.63
1D-PWF + IWF	21.29	0.45	23.17	0.67
1D-PWF + SWF	21.31	0.45	23.18	0.67
AT-GWF + NLM	21.03	0.42	23.45	0.54
AT-GWF + BM3D	**21.96**	0.48	**26.40**	0.68
AT-GWF + 2D-PWF	21.44	0.43	24.45	0.59
AT-GWF + GWF	21.32	0.44	25.62	0.66
AT-GWF + IWF	21.30	0.45	26.09	**0.69**
AT-GWF + SWF	21.32	0.45	26.16	**0.69**
AT-IWF + NLM	20.89	0.42	20.26	0.48
AT-IWF + BM3D	21.78	0.47	22.52	0.65
AT-IWF + 2D-PWF	21.26	0.43	20.62	0.52
AT-IWF + GWF	21.33	0.45	22.11	0.63
AT-IWF + IWF	21.41	0.46	22.40	0.65
AT-IWF + SWF	21.43	0.46	22.41	0.65
AT-SWF + NLM	20.45	0.42	20.64	0.50
AT-SWF + BM3D	21.14	0.47	22.84	0.67
AT-SWF + 2D-PWF	20.78	0.43	21.10	0.55
AT-SWF + GWF	20.69	0.44	22.42	0.65
AT-SWF + IWF	20.57	0.44	22.58	0.66
AT-SWF + SWF	20.58	0.45	22.59	0.66

In practice, we notice a lower processing time when denoising a CT image with double-filtering and FBP, comparing with state-of-art iterative reconstruction methods which use slow reconstruction algorithms, as Projections Onto Convex Sets (POCS) [17]. Therefore, a double-filtering which uses a fast reconstruction algorithm, as FBP, can become a powerful tool in order to get a better balance between details preservation and noise reduction in CT.

Finally, for a future work we can consider double-filtering using other methods, also a *time vs. quality* comparison between double-filtering (using FBP) and iterative reconstruction methods, and even new patch shapes for BM3D in pre-filtering step.

ACKNOWLEDGMENTS

The authors are grateful to São Paulo Research Foundation - FAPESP (grants 2013/25595-7 and 2014/11964-3) for the financial support in our projects and to Prof. Dr. Paulo Estevão Cruvinel (Brazilian Corporation of Agricultural Research - EMBRAPA) for providing the images for study.

REFERENCES

[1] A. C. Kak and M. Slaney, *Principles of computerized tomographic imaging*. New York: IEEE Press, 1988.

[2] C. L. Epstein, *Introduction to the mathematics of medical imaging*, 2nd ed. Philadelphia, PA: Society for Industrial and Applied Mathematics, 2008.

[3] C. Deledalle, F. Tupin, and L. Denis, "Poisson NL means: Unsupervised non local means for poisson noise," *17th IEEE International Conference on Image Processing (ICIP)*, pp. 801–804, 2010.

[4] D. H. P. Salvadeo, "Filtragem de ruído em imagens tomográficas com baixa taxa de contagem utilizando uma abordagem bayesiana contextual," Ph.D. dissertation, UFSCar, São Carlos, 2013 (in portuguese).

[5] M. A. M. Laia, A. L. M. Levada, L. C. Botega, M. F. L. Pereira, P. E. Cruvinel, and Á. Macedo, "A novel model for combining projection and image filtering using kalman and discrete wavelet transform in computerized tomography," *11th IEEE International Conference on Computational Science and Engineering*, pp. 219–226, 2008.

[6] J. Ma, J. Huang, Z. Liang, H. Zhang, Y. Fan, Q. Feng, and W. Chen, "Image fusion for low-dose computed tomography reconstruction,," *IEEE Nuclear Science Symposium and Medical Imaging Conference (NSS/MIC)*, pp. 4239,4243, 2011.

[7] F. J. Anscombe, *The Transformation of Poisson, Binomial and Negative-Binomial Data*, 35th ed., Biometrika, December 1948.

[8] E. S. Ribeiro, "Novas propostas em filtragem de projeções tomográficas sob ruído poisson," Master's thesis, UFSCar, São Carlos, 2010 (in portuguese).

[9] D. T. Kuan, A. A. Sawchuk, T. C. Strand, and P. Chavel, "Adaptive noise smoothing filter for images with signal-dependent noise," *IEEE Trans. Pattern Anal. Mach. Intell.*, vol. 7, no. 2, pp. 165–177, 1985.

[10] A. Buades, B. Coll, and J. M. Morel, "A review of image denoising algorithms, with a new one," *Simul*, vol. 4, pp. 490–530, 2005.

[11] K. Dabov, A. Foi, V. Katkovnik, and K. Egiazarian, "Image denoising by sparse 3d transform-domain collaborative filtering," *IEEE Transactions on Image Processing*, vol. 16, no. 8, p. 2080, 2007.

[12] A. L. M. Levada and N. D. A. Mascarenhas, "Filtragem adaptativa de ruído gaussiano em imagens através da minimização da informação de fisher observada," *VI Workshop de Visão Computacional (WVC'2010)*, pp. 7–12, 2010 (in portuguese).

[13] S. M. Kay, *Fundamentals of Statistical Signal Processing: Estimation Theory*. Upper Saddle River, NJ, USA: Prentice-Hall, Inc., 1993.

[14] M. Mäkitalo and A. Foi, "Optimal inversion of the anscombe transformation in low-count poisson image denoising," *IEEE Transactions on Image Processing*, vol. 20, no. 1, pp. 99–109, 2011.

[15] S. Peltonen, U. Tuna, and U. Ruotsalainen, "Low count pet sinogram denoising," *Nuclear Science Symposium and Medical Imaging Conference (NSS/MIC)*, pp. 3964–3967, 2012.

[16] Z. Wang and A. C. Bovik, "Mean squared error: Love it or leave it?" 2009.

[17] F. V. Salina, "Métodos híbridos para reconstrução tomográfica de imagens usando pocs e teoria da estimação," Ph.D. dissertation, IFSC/USP, São Carlos, 2007 (in portuguese).

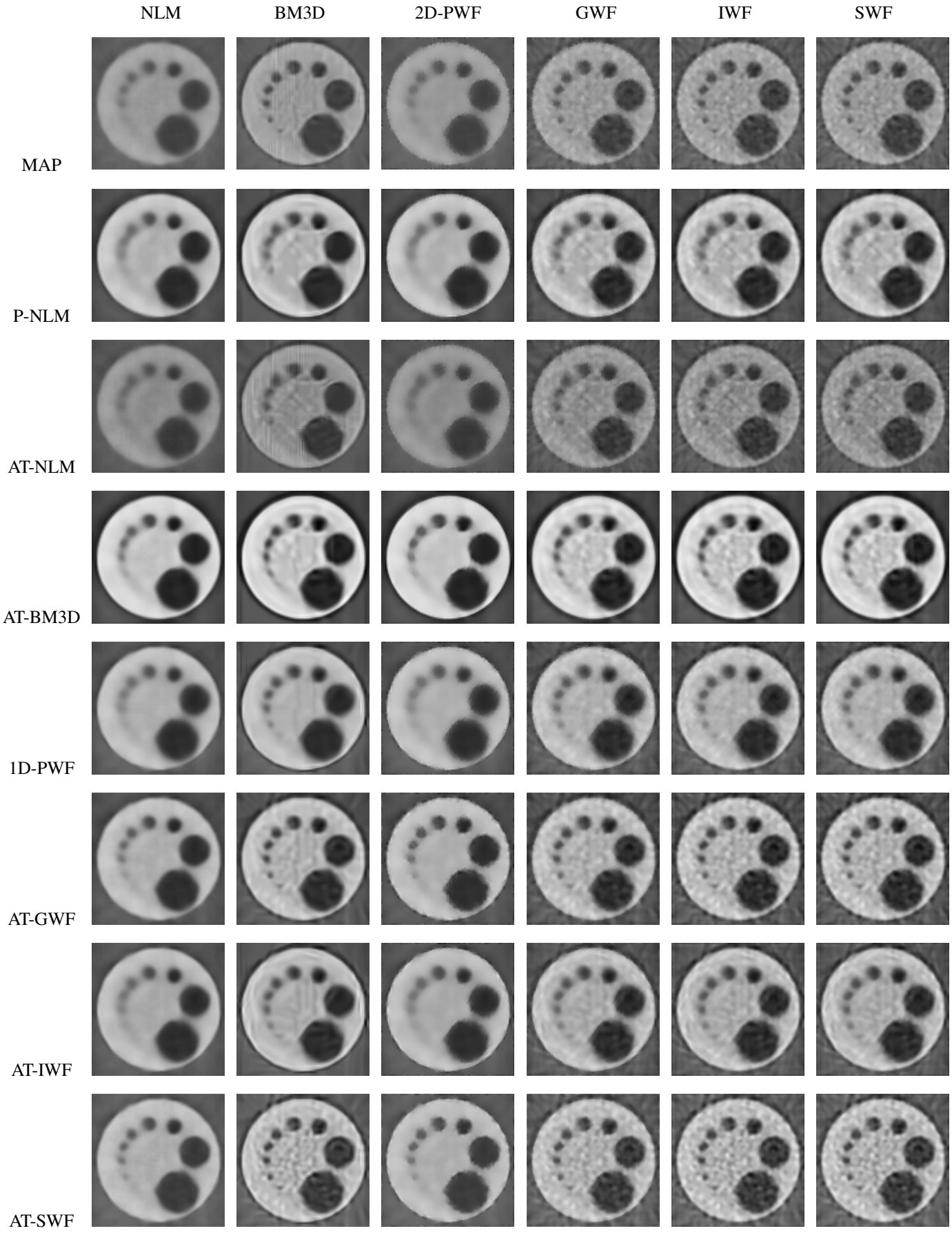

Fig. 6. Results of double denoising for Image 1

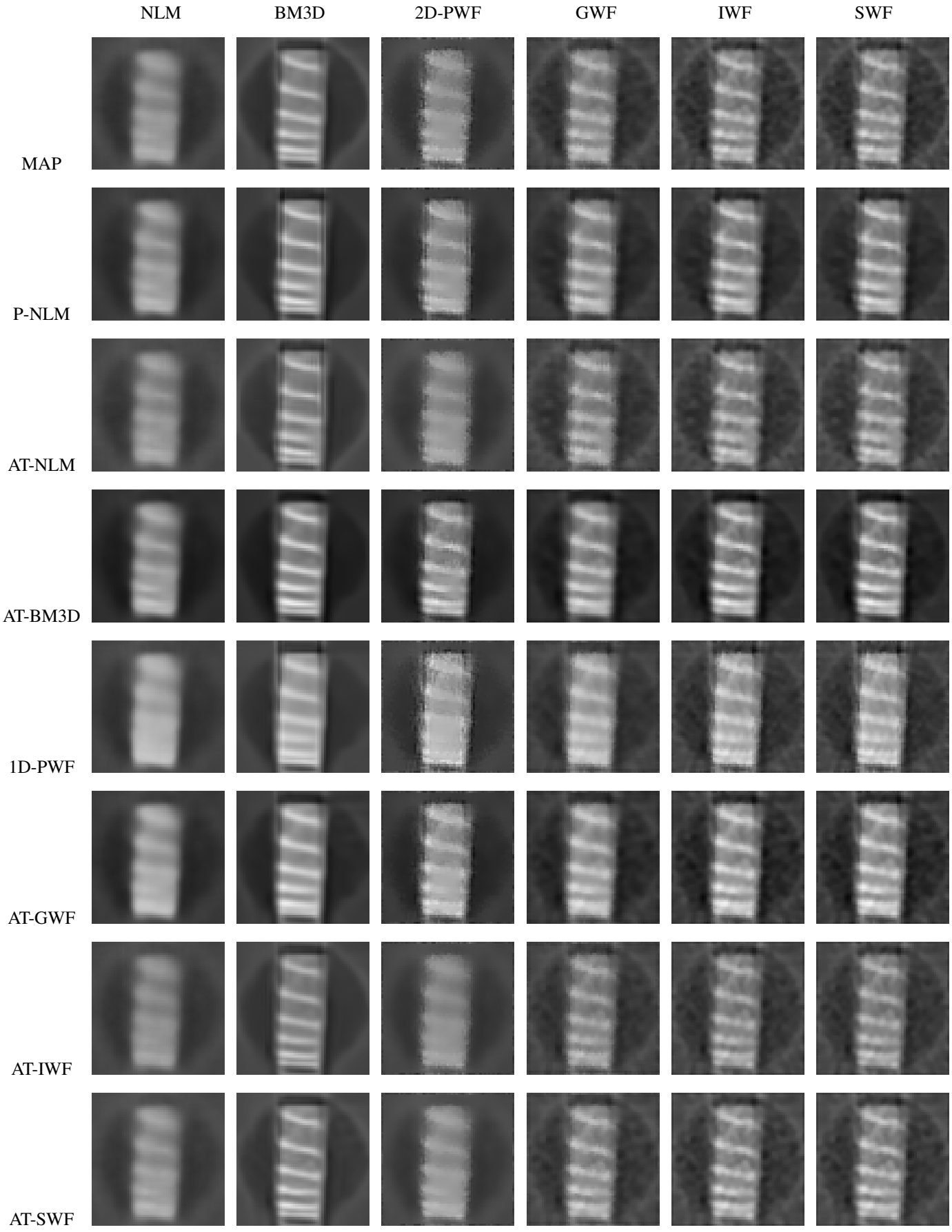

Fig. 7. Results of double denoising for Image 2